

NuSTAR and *XMM–Newton* observations of the Arches cluster in 2015: fading hard X-ray emission from the molecular cloud

Roman Krivonos^{1*}, Maïca Clavel², JaeSub Hong³, Kaya Mori⁴, Gabriele Ponti⁵

Juri Poutanen^{6,7}, Farid Rahoui^{8,9}, John Tomsick² and Sergey Tsygankov⁶

¹Space Research Institute of the Russian Academy of Sciences, Profsoyuznaya Str. 84/32, 117997 Moscow, Russia;

²Space Sciences Laboratory, 7 Gauss Way, University of California, Berkeley, CA 94720-7450, USA;

³Harvard-Smithsonian Center for Astrophysics, 60 Garden Street, Cambridge, MA 02138, USA;

⁴Columbia Astrophysics Laboratory, Columbia University, New York, NY 10027, USA;

⁵Max-Planck-Institut für extraterrestrische Physik, Giessenbachstrasse 1, Garching, 85748, Germany;

⁶Tuorla Observatory, Department of Physics and Astronomy, University of Turku, Väisäläntie 20, FI-21500 Piikkiö, Finland;

⁷Nordita, KTH Royal Institute of Technology and Stockholm University, Roslagstullsbacken 23, SE-10691 Stockholm, Sweden;

⁸European Southern Observatory, Karl-Schwarzschild-Str. 2, D-85748 Garching bei München, Germany;

⁹Harvard University, Department of Astronomy, 60 Garden street, Cambridge, MA 02138, USA;

13 December 2016

ABSTRACT

We present results of long *NuSTAR* (200 ks) and *XMM–Newton* (100 ks) observations of the Arches stellar cluster, a source of bright thermal ($kT \sim 2$ keV) X-rays with prominent Fe XXV $K\alpha$ 6.7 keV line emission and a nearby molecular cloud, characterized by an extended non-thermal hard X-ray continuum and fluorescent Fe $K\alpha$ 6.4 keV line of a neutral or low ionization state material around the cluster. Our analysis demonstrates that the non-thermal emission of the Arches cloud underwent a dramatic change, with its homogeneous morphology, traced by fluorescent Fe $K\alpha$ line emission, vanishing after 2012, revealing three bright clumps. The declining trend of the cloud emission, if linearly fitted, is consistent with half-life decay time of ~ 8 years. Such strong variations have been observed in several other molecular clouds in the Galactic Centre, including the giant molecular cloud Sgr B2, and point toward a similar propagation of illuminating fronts, presumably induced by the past flaring activity of Sgr A*.

Key words: ISM: clouds, X-rays: individual (Arches cluster)

1 INTRODUCTION

The Arches cluster is a massive star cluster with a core that is about $9''$ (~ 0.35 pc at 8 kpc) in radius (Figer et al. 1999), containing more than 160 O-type stars (Figer et al. 2002). It is located in the inner Galactic Center (GC) region at the projected angular distance of $11'$ from Sgr A*. *Chandra* observations of the Arches cluster region revealed a complicated picture of the X-ray emission, showing the presence of spatially separated thermal and non-thermal emission components. The thermal emission is thought to originate in the cluster’s core from multiple collisions between strong winds of massive stars (Yusef-Zadeh et al. 2002; Wang et al. 2006;

Capelli et al. 2011a). Diffuse non-thermal X-ray emission has been detected from a broad region (“clouds”) around the cluster (Wang et al. 2006; Tsujimoto et al. 2007; Capelli et al. 2011b; Tatischeff et al. 2012; Krivonos et al. 2014). The non-thermal nature of this extended radiation is revealed by its strong fluorescent Fe $K\alpha$ 6.4 keV line emission, presumably coming from material that is neutral or in a low ionization state.

Two physical mechanisms to produce fluorescent emission in the molecular clouds are generally discussed. The first implies reflection of incoming hard X-rays where K-shell photoionization and the subsequent fluorescence produce a strong Fe $K\alpha$ line with an equivalent width $EW \gtrsim 1$ keV (Sunyaev, Markevitch, & Pavlinsky 1993; Markevitch, Sunyaev, & Pavlinsky 1993; Koyama et al. 1996; Sunyaev & Churazov

* E-mail: krivonos@iki.rssi.ru

1998). Additionally, the Compton scattering of high-energy photons results in a reflection hump around 20–30 keV. The source of the incoming X-rays might be associated with a nearby X-ray source (e.g. Churazov et al. 1993, 1E1740.7-2942) or with past activity of Sgr A*, as suggested by Sunyaev, Markevitch, & Pavlinsky (1993) to explain the hard X-ray emission of the giant molecular cloud Sgr B2 in the GC region, leading to prediction of the bright 6.4 keV line later confirmed by the observations (Koyama et al. 1996; Sunyaev & Churazov 1998; Murakami et al. 2000; Revnivtsev et al. 2004; Terrier et al. 2010; Zhang et al. 2015). A long outburst from Sgr A* lasting more than 10 years and ending a few hundred years ago could explain the Sgr B2 emission (Koyama et al. 1996; Terrier et al. 2010). The hypothesis of past Sgr A* flaring activity is supported by the discovery of a propagation of Fe K echos in the Central Molecular Zone (CMZ), presumably from a source far away from the clouds (Ponti et al. 2010, 2013; Clavel et al. 2013; Ryu et al. 2013). Alternative explanation suggests the propagation of cosmic-ray (CR) particles within the molecular clouds, which can produce hard X-rays and Fe K α emission (Valinia et al. 2000; Dogiel et al. 2009; Tatischeff et al. 2012; Dogiel et al. 2014), however CR scenarios fail to reproduce the fast variability that is observed in numerous clouds of the CMZ (Terrier et al. 2017).

Based on the archival *XMM* data of the GC region, Capelli et al. (2011b) and Tatischeff et al. (2012) constructed Fe K α emission line maps of the Arches cluster region at 6.4 keV and showed that this emission extends well beyond the cluster’s core. Capelli et al. (2011b) argue that the observed Fe K α line flux and the high value of the equivalent width ($EW_{6.4 \text{ keV}}$) suggest an origin of the fluorescence in the photoionization of the cloud by X-ray photons, although excitation by CR is not specifically excluded. Tatischeff et al. (2012) (hereafter T12) suggested that the Fe K α 6.4 keV line emission observed around the Arches cluster is likely produced by bombardment of molecular gas by low-energy cosmic-ray protons (LECR p). The authors suggest that the required large flux of low-energy CR particles could be produced in the ongoing supersonic collision between the star cluster and a nearby molecular cloud.

Using the first hard X-ray focused observation of the Arches cluster region, performed with *NuSTAR*, we showed in our previous work (Krivonos et al. 2014, hereafter K14) that the continuum emission in the 10–20 keV band is significantly detected around the Arches cluster with a spatial morphology consistent with the Fe K α fluorescent line emission.

Clavel et al. (2014, hereafter C14) analysed the long-term behavior of the Arches cluster cloud (or simply the Arches cloud) over 13 years and reported a 30% decrease (4σ confidence) in Fe K α line and continuum flux of the cloud emission, providing significant evidence for the X-ray reflection scenario. Despite this success, the question of determining the illuminating hard X-ray source and reflection geometry remains open. The source cannot be within the Arches cluster, according to constraints drawn from the Fe K α line flux (T12) and hard X-ray continuum (K14), leaving the possibility for putative past activity of Sgr A*. In this work we track further the evolution of the flux of the Fe K α line with *XMM-Newton* observations and measure the shape of the hard X-ray continuum with *NuSTAR*.

Table 1. List of the X-ray observations of the Arches cluster with *XMM-Newton* and *NuSTAR* used in this work

Mission	Date	ObsID	Exp. (ks)	Frac.* (%)
<i>XMM-Newton</i>	2015-09-27	0762250301	112.0	78/84/60
<i>NuSTAR</i>	2015-10-19	40101001002	107.2	100/0
<i>NuSTAR</i>	2015-10-25	40101001004	107.8	100/0

*Good time fraction for *XMM-Newton* MOS1/MOS2/PN and *NuSTAR* FPMA/FPMB, respectively; Note that *NuSTAR* FMPB data were completely rejected due to stray-light contamination (Sect. 2.2).

Although the CR-only scenario is practically ruled out by the observed variability for most of the measured non-thermal emission, the origin of the remaining faint emission is not so obvious. As the non-thermal flux decreases, we might now be observing a significant contribution from a putative steady background level, which could be created by a different process than the one responsible for the bulk of variable emission. In this paper, we repeat the spectral fit performed by K14 to derive updated constraints for both the X-ray photoionization and the LECR emission models based on the spectral shape above 10 keV using the *NuSTAR* data taken in 2015.

The paper is structured as follows. In Sect. 2 we describe observations of the Arches cluster with *XMM-Newton* and *NuSTAR* in 2015 and outline the corresponding data analysis. Spectral modelling of the Arches cluster core and cloud emission is presented in Sect. 3. Discussion of the results obtained and the summary can be found in Sect. 4 and 5, respectively. Additional materials (e.g., serendipitous detection of the Sgr A complex and a description of 2D image spectral extraction procedure) are placed in the Appendix.

2 OBSERVATIONS AND DATA ANALYSIS

2.1 *XMM-Newton*

The *XMM-Newton* data reduction was carried out using the *XMM-Newton* Extended Source Analysis Software (ESAS, Snowden et al. 2008) included in version 14 of the *XMM-Newton* Science Analysis Software (SAS). We followed the procedure described by C14, using the SAS *emchain* and *epchain* scripts to produce the calibrated event lists and ESAS mos-filter and pn-filter to exclude periods affected by soft proton flaring.

The *XMM-Newton* source and astrophysical background spectra were extracted from these clean event lists with the ESAS *mos-spectra* and *pn-spectra* tasks. For the ‘Cloud’ region, we also extracted the corresponding quiescent particle background (QPB) from the filter wheel closed event lists provided by the ESAS calibration database and normalized them to the level of QPB in the observations, using *pn_back* and *mos_back*. Spectrum counts were grouped to have at least thirty counts per bin so that we can validly use chi-squared statistics for fitting (Sect. 3).

To produce the continuum-subtracted images we fol-

Table 2. Definitions of the sky regions.

RA (J2000)	Dec (J2000)	Parameters
Cluster (circle)		
17 ^h 45 ^m 50.3 ^s	−28°49′19″	15″
Cloud (ellipse)		
17 ^h 45 ^m 51.0 ^s	−28°49′16″	25″, 59″, 155°
17 ^h 45 ^m 50.3 ^s	−28°49′19″	15″ (excl.)
Arches cluster complex (circle)		
17 ^h 45 ^m 50.3 ^s	−28°49′19″	50″
Background (annulus)		
17 ^h 45 ^m 50.3 ^s	−28°49′19″	130″
17 ^h 45 ^m 50.3 ^s	−28°49′19″	70″ (excl.)

Notes. Central position and radius for circular regions, and semi-minor/major axes and rotation angle for the elliptical regions. The rotation is defined counter clockwise relative to North (upward). Background region is shown in Fig. 2. “Cluster” and “Cloud” regions are illustrated in Fig. 1. The excluded regions are marked as “excl.”.

lowed the optimized procedure presented by Terrier et al. (2017), which can be summarized as follow. For each instrument we produced the count, background and exposure maps with initial resolution of 2.5 arcsec, using *mos_spectra*, *pn_spectra*, *mos_back* and *pn_back* in three energy bands: 4.7–6.3, 6.32–6.48 and 6.62–6.78 keV. To estimate the continuum underlying the emission lines we assumed the following spectral model: a power-law of photon index $\Gamma = 2$ plus a thermal plasma of temperature $kT = 6.5$ keV (with abundance equal to solar), both components being absorbed by a column density $N_{\text{H}} = 7 \times 10^{22} \text{ cm}^{-2}$. For each pixel, the normalizations of these two components were derived using the continuum emission within 4.7–6.3 keV and the line+continuum emission at 6.7 keV, allowing to subtract both the continuum emission underlying the 6.4 keV line and the non-thermal emission underlying the 6.7 keV line. After taking into account the different efficiencies of the three EPIC detectors, the individual instrument maps were then combined to create the corresponding continuum-subtracted flux maps. Fig. 1 shows Fe K α images at 6.4 keV and 6.7 keV obtained, respectively, in 6.32–6.48 keV and 6.62–6.78 keV energy bands. As expected, the cluster’s core is bright at 6.7 keV line revealing strong thermal radiation in the stellar cluster.

The Arches cluster core thermal emission located within the circular region of $R \sim 15''$ is embedded in the elongated non-thermal emission of the cloud with dimensions of $\sim 25'' \times 59''$. In order to perform spatial and spectral analysis consistent with recent studies of the Arches cluster region (T12, K14, C14), we adopt the same sky regions to describe the core of the Arches cluster and the surrounding cloud region listed in Table 2. The cloud region is represented by an ellipse excluding the circular region of the cluster’s core.

2.2 *NuSTAR*

The *Nuclear Spectroscopic Telescope Array* (*NuSTAR*) hard X-ray orbital telescope (Harrison et al. 2013) provides arcminute angular resolution imaging at energies above 10 keV

not accessible by any previously or currently operating missions. *NuSTAR* carries two identical co-aligned X-ray telescopes with an angular resolution of 18″ (full width at half maximum, FWHM). The focal plane detector units of each telescope, referred to as focal plane module A and B (FPMA and FPMB), cover a wide energy band 3–79 keV, and provide spectral resolution of 400 eV (FWHM) at 10 keV.

The Arches cluster was serendipitously observed during the Galactic Center (GC) region campaign (Mori et al. 2015) with the *NuSTAR* in 2012 October. Despite the fact that the Arches was observed at high off-axis angle, i.e. with low efficiency, K14 showed that the continuum 10–20 keV emission at that time was significantly detected around the Arches cluster with a spatial morphology consistent with the Fe K α fluorescent line emission. To better constrain the spectrum, morphology and variability of the hard X-ray non-thermal emission of the Arches cluster, we initiated the dedicated on-axis observations performed in 2015 with the total exposure of 200 ks.

The *NuSTAR* detectors can register X-rays passing outside the X-ray optics modules due to gaps in detector shielding (see e.g. Wik et al. 2014; Mori et al. 2015). Unfocused flux of direct (“zero-bounce”) photons or so called “stray-light” can be a significant contributor to the detector background if there are bright X-ray sources within 2–5 deg of the *NuSTAR* field of view (FOV). Examining FPMB data, we noticed strong stray-light contamination from the bright X-ray source GX 3+1 (Seifina & Titarchuk 2012) covering the Arches cluster region, which led to rejection of FPMB data in the following analysis. In addition to that FPMA data taken in 2015 were contaminated by ghost-rays (“one bounce” photons) from two nearby bright sources. The visible ghost-ray patterns are consistent with the position of persistent X-ray source 1E 1743.1-2843 (see e.g. Lotti et al. 2016, and references therein) and transient LMXB AX J1745.6-2901, which started its prolonged outburst in 2013 July (Degenaar et al. 2015; Ponti et al. 2015) and faded in 2016 (Degenaar et al. 2016). Nevertheless, the Arches cluster core and cloud are not strongly contaminated and can be well localized in FPMA images as obviously seen in Fig. 2, and also based on actual ghost-rays seen in other *NuSTAR* observations (Bodaghee et al. 2014).

Note that the celestial coordinates of each photon registered with *NuSTAR* are determined with some uncertainty caused by thermal bending and external forces acting on the mast during orbit. The systematic shift of the source position can be as high as 10″. We noticed an offset of the cluster core in 2015 data at the level of $\sim 4''$. Since the first *NuSTAR* serendipitous observation of the Arches cluster taken in 2012 demonstrated good agreement between the position of the cluster core and bright *Chandra* sources in it, we use core centroid coordinates R.A.=17^h45^m50.52^s, Dec.=−28°49′23.07″ measured in K14 as a reference position¹ to correct sky coordinates of each incoming photon in 2015 data set.

The angular separation of the Arches cluster’s core and

¹ Note that Table 3 in K14 contains mistaken centroid position of the Arches cluster core, the coordinates R.A.=17^h50^m50.43^s, Dec.=−28°49′23.07″ should be read as R.A.=17^h45^m50.52^s, Dec.=−28°49′22.41″.

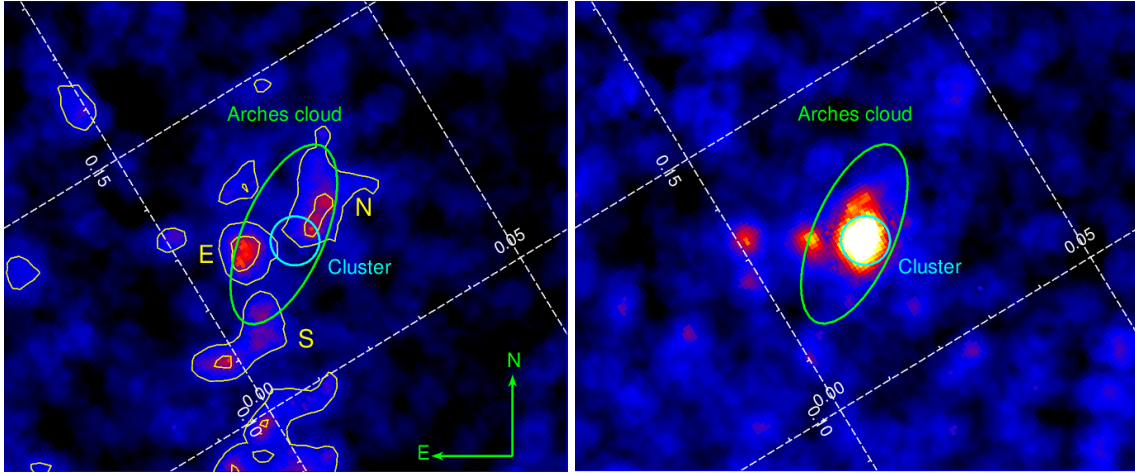


Figure 1. *XMM-Newton* $K\alpha$ line mosaic image of the Arches cluster region of the iron at 6.4 keV (left) and 6.7 keV (right) obtained in 6.32–6.48 and 6.62–6.78 keV energy bands, respectively. The images are continuum subtracted and adaptively smoothed. The contours in the left image are shown to highlight bright clumps of 6.4 keV emission. The compass sign shows the images alignment in equatorial coordinates, with North up and East to the left.

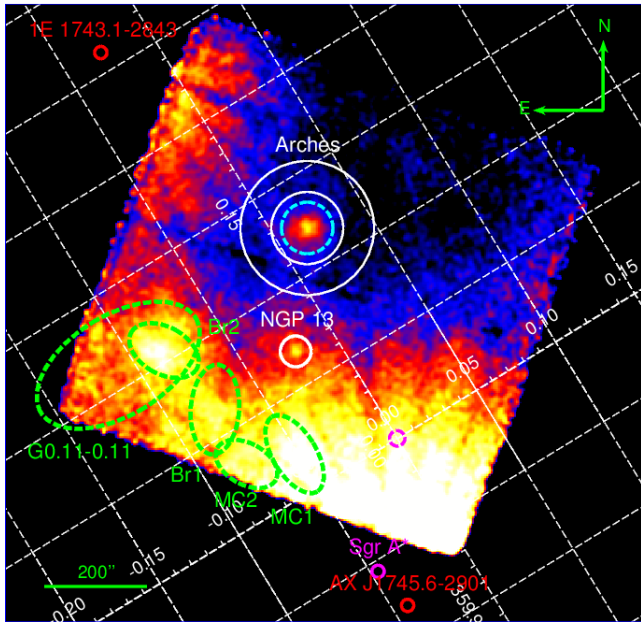


Figure 2. *NuSTAR* image of the Arches cluster region in 3–79 keV energy band based on FPMA data only. The image is based on two *NuSTAR* observations and comprises 215 ks of exposure time. The position of the Arches cluster is shown by the cyan circle ($R = 50''$) marked in a dashed style. The source and background spectrum are extracted, respectively, from the same green circle and annulus region ($R_{\min} = 70''$, $R_{\max} = 130''$). The sources of ghost-ray contamination are marked in red. Green sky regions reveal positions of selected Sgr A molecular clouds (Clavel et al. 2013). NGP 13 denotes position of an X-ray point source from the *NuSTAR* survey of the Galactic center region (Hong et al. 2016), also being a counterpart of the *Chandra* point source CXOUGC J174551.9–285311 (Muno et al. 2009). Magenta circle shows the center of the Galactic coordinates.

cloud is sufficient to spatially resolve these emission components with *NuSTAR*. However, spectral analysis of the given area is seriously complicated due to the wide wings of the *NuSTAR* PSF: the corresponding half-power diameter (HPD, enclosing half of the focused X-rays), reaches $\sim 60''$ (Madsen et al. 2015), which causes partial confusion of the Arches cluster and its cloud. Taking the above into account, we extract the spectrum of the Arches cluster from a circular region with $R = 50''$ pointed at the cluster centroid position, covering both the cluster core and the cloud. The spectrum was extracted using the *nuproducts* task of the *NuSTAR* Data Analysis Software (NUSTARDAS) v.1.5.1 and HEASOFT v6.17. The background spectrum was extracted from the annulus region within the radii range $R = 70 - 130''$, chosen as a result of a trade-off between the representative background and ghost-ray contamination.

3 SPECTRAL MODELING

In this section we describe the details of our spectral analysis of the different regions of the Arches cluster, namely: i) the core of the stellar cluster within $R = 15''$ circular region; ii) the cloud ellipse region; and iii) the circular area of $R=50''$ containing both cluster core and cloud, also referred later as ‘the Arches cluster complex’ (for the region coordinates see Table 2). We first analyse *XMM-Newton* and *NuSTAR* data alone, comparing with previous observations and constructing the time evolution of the cloud non-thermal emission, then we present the first *XMM-Newton* and *NuSTAR* broadband joint spectral fit of the Arches cluster complex, and finally perform 2D image analysis to separate stellar cluster and cloud emission. The uncertainty estimates of the fitted model parameters in the following discussion are shown at the 90% confidence level.

We begin with spectral analysis of the Arches core emission to check the consistency of its spectral shape with previous observations and to validate our data reduction procedures.

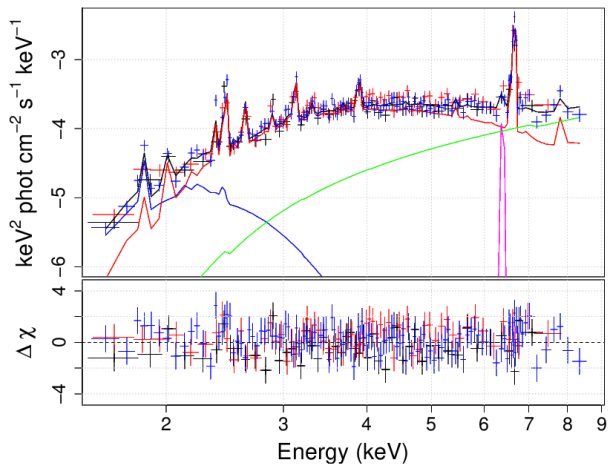


Figure 3. X-ray spectrum of the Arches cluster based on the long *XMM–Newton* observation performed in 2015. The spectrum was extracted from $R = 15''$ circular region (Table 2). MOS1, MOS2, and PN data are shown in black, red, and blue colors, respectively. The fitted model includes two APEC components with $kT = 0.22^{+0.08}_{-0.05}$ keV (blue) and $kT = 1.58^{+0.13}_{-0.09}$ keV (red), and non-thermal power-law continuum (green) with Gaussian 6.4 keV line coloured in magenta (Model 2 in Table 3). Hereafter, all spectra are shown in logarithmic scale, with Y axis labelled with only the exponents.

3.1 XMM–Newton: Cluster emission

We extracted the spectrum of the Arches cluster from a $15''$ circular region and the corresponding instrumental and astrophysical background from an annulus region around the cluster (Table 2). The Arches cluster X-ray emission, which likely originates in one or more extreme colliding wind massive star binaries (Capelli et al. 2011a), is dominated by a thermal emission with prominent iron 6.7 keV line, however, at the same time, contribution from X-ray bright clouds is not negligible. We thus model the emission of the cluster region with an APEC plasma component and a non-thermal component composed by a power-law continuum and Fe 6.4 keV line. All the spectral emission components were subject to interstellar photo-electric absorption modelled with *wabs* in *XSPEC*. APEC thermal plasma model is characterized by kT , Z/Z_{\odot} , and I_{kT} parameters, respectively, describing temperature, metallicity relative to solar, and normalization in units of $10^{-18} \int n_e n_H dV / (4\pi D^2)$, where n_e and n_H are the electron and proton number densities in units of cm^{-3} , and D is the cluster distance in cm. Based on the previous observations of the Arches cluster with *XMM–Newton* (T12, Wang et al. 2006) we fixed the metallicity to $Z = 1.7Z_{\odot}$ throughout the paper. The best-fitting parameters of the current model are summarized in Table 3 and the corresponding MOS1/MOS2/PN spectra are shown in Fig. 3. Note, that we also fixed the energy of the 6.4 keV line due to its low flux relative to the bright 6.7 keV line, which cause systematic shift towards higher energies.

The value of N_H is higher than the Galactic value in the direction to the Arches cluster ($N_H = 1.2 \times 10^{22} \text{ cm}^{-2}$; Kalberla et al. 2005), by an order of magnitude, which indicates strong local absorption, most likely caused both

Table 3. Best-fitting spectral model parameters for the Arches cluster core emission ($R = 15''$ circular region) measured with *XMM–Newton*.

Parameter	Unit	Model 1*	Model 2**
N_H	10^{22} cm^{-2}	8.73 ± 0.50	11.23 ± 1.00
kT	keV		$0.22^{+0.08}_{-0.05}$
I_{kT}	(see Sect. 3.1)		$1.91^{+16.61}_{-1.62} \times 10^3$
kT	keV	1.82 ± 0.10	$1.58^{+0.13}_{-0.09}$
I_{kT}	(see Sect. 3.1)	13.60 ± 2.00	22.54 ± 5.00
$E_{6.4 \text{ keV}}$	keV	6.4 (fixed)	6.4 (fixed)
$N_{6.4 \text{ keV}}$	$10^{-7} \text{ ph cm}^{-2} \text{ s}^{-1}$	$1.82^{+3.47}_{-1.82}$	$1.55^{+3.62}_{-1.55}$
Γ		1.13 ± 0.70	0.33 ± 1.00
I_{pow}	$10^{-5} \text{ cm}^{-2} \text{ s}^{-1} \text{ keV}^{-1}$	$1.86^{+4.07}_{-1.42}$	$0.38^{+1.93}_{-0.34}$
$\chi^2_{\text{r}}/\text{d.o.f.}$		1.13/240	1.05/238

*) WABS \times (APEC + Gaussian + power law);

**) WABS \times (APEC + APEC + Gaussian + power law);

by strong stellar winds of massive stars in the cluster and nearby molecular material of the cloud. The temperature of the thermal emission $kT = 1.82 \pm 0.10$ keV is consistent with the previous measurement (T12, Capelli et al. 2011a). The hard power-law continuum $\Gamma \sim 1$ emission is also in agreement with that found in previous studies. However, the uncertainties, mainly caused by the low statistics and the soft energy range $E < 10$ keV, are large. Capelli et al. (2011a) reported on 70% brightening of the Arches cluster emission in March/April 2007 relative to an average level of $F_{2-10 \text{ keV}} = 1.5 \pm 0.1 \times 10^{-12} \text{ erg s}^{-1} \text{ cm}^{-2}$ (2–10 keV, absorption corrected). Using the *cflux* model in *XSPEC* we estimated a 2–10 keV unabsorbed total flux of the cluster of $F_{2-10 \text{ keV}} = 1.50^{+0.30}_{-0.25} \times 10^{-12} \text{ erg s}^{-1} \text{ cm}^{-2}$, which is fully consistent with the normal state flux level reported by Capelli et al. (2011a).

The second APEC component emission ($kT \sim 0.2$ keV) which could be due to a collection of individual stars, as suggested by T12, significantly improves the fit statistics (expressed by reduced $\chi^2_{\text{r}} = 1.05$ for 238 degrees of freedom, d.o.f.). In contrast to T12, introducing separate absorber for the soft component of the cluster emission did not provide an improvement to the fit ($\chi^2_{\text{r}}/\text{d.o.f.} = 1.15/237$), which is most likely caused by the low sensitivity to the soft spectral component of our data set, based on lower exposure compared to that used by T12.

3.2 XMM–Newton: Cloud emission

In this section we describe the spectral analysis of the cloud emission based on the data taken during the long *XMM–Newton* observation on September 27, 2015. The main question we address here is the evolution of the cloud non-thermal emission since 2012, when a drop was detected as reported by C14. Strong variation implies that a large fraction of the non-thermal emission of the cloud is due to the reflection of an X-ray transient source.

To track the evolution of the cloud emission in a way

that is consistent with previous works (T12, C14), we extract *XMM-Newton* spectrum from $25'' \times 59''$ ellipse region excluding the cluster emission (Table 2). Following C14 we consider the 2–7.5 keV energy range and spectral model $wabs \times (apec + powerlaw) + gaussian$, fixing the temperature of the *apec* plasma component to the $kT = 2.2$ keV, metallicity to $Z = 1.7Z_{\odot}$, the power-law index to $\Gamma = 1.6$, the centroid energy and width of the gaussian to 6.4 keV and 10 eV, respectively (C14). Due to the low statistics of the cloud region and the limited energy range selected (2–7.5 keV), the 2.2 keV *apec* component represents an average temperature plasma at the position of the cloud, accounting for the soft and hard thermal diffuse emission components at 1 and 7 keV, usually considered to model the thermal background at the GC (e.g. Munro et al. 2004). For this specific analysis, we used the *XMM-Newton* instrumental background as described in C14. The best-fitting parameters of this model obtained in the 2–7.5 keV energy interval are listed in Table 5 (Model 1). Note that the fit is relatively poor ($\chi^2_r/d.o.f. = 1.54/224$), mainly due to the strong line excess at ~ 2.45 keV, presumably belonging to $K\alpha$ line from He-like Sulfur (S). We first tried to add a low-temperature thermal emission component, however this approach: i) did not remove the line at ~ 2.45 keV, and hence ii) did not improve the fit statistics; and iii) introduced the significant deviation relative to C14 method, making it difficult to compare with the long-term evolution of the cloud observed by C14. Therefore, we follow an ‘ad-hoc’ approach described as follows. Since the continuum of low thermal emission was already taken into account by an average 2.2 keV *apec* plasma component, we extended the spectral model by adding a Gaussian line at ~ 2.45 keV (Model 2 in Table 5). Model 2 provides a better fit statistics ($\chi^2_r/d.o.f. = 1.21/222$) and it does not significantly change the parameters of the non-thermal component (Table 5). This allows us to directly compare with the C14 lightcurve of the Arches cloud both in the 6.4 keV line emission and the power-law continuum.

C14 pointed out that the overall absorption and normalization of the thermal plasma are compatible with being constant over the 13-year (2001–2014) period with the estimated weighted mean values of $N_H = 6.0 \pm 0.3 \times 10^{22} \text{ cm}^{-2}$ and $I_{2.2 \text{ keV}} = 3.6 \pm 0.7 \times 10^{-4} \text{ cm}^{-5}$, respectively. Our fitting procedure gives a comparable absorption and a marginally higher plasma normalization $I_{2.2 \text{ keV}}$.

The equivalent width of the Fe 6.4 keV emission line was calculated with respect to the power-law continuum using the task *equwidth* in *SHERPA* package (Freeman et al. 2001), a part of the CIAO-4.7 software (Fruscione et al. 2006). C14 showed that the equivalent width of the Fe $K\alpha$ line is compatible with being constant over time with an average value $EW = 0.9 \pm 0.1$ keV (also consistent with other studies Capelli et al. 2011b, T12, K14), indicating that most of the power-law continuum is linked to the 6.4 keV emission. Our results obtained from the new 2015 *XMM-Newton* observations show that the line strength decreased to $EW = 0.6 - 0.7$ keV (see Table 5).

The overall evolution of the normalizations of the 6.4 keV line and the reflection continuum is shown in Fig. 5, where the declining trend of the non-thermal emission of the Arches cloud is clearly seen. Comparing the current normalizations of the Fe 6.4 keV line and the power-law continuum with the average emission up to 2011 as reported

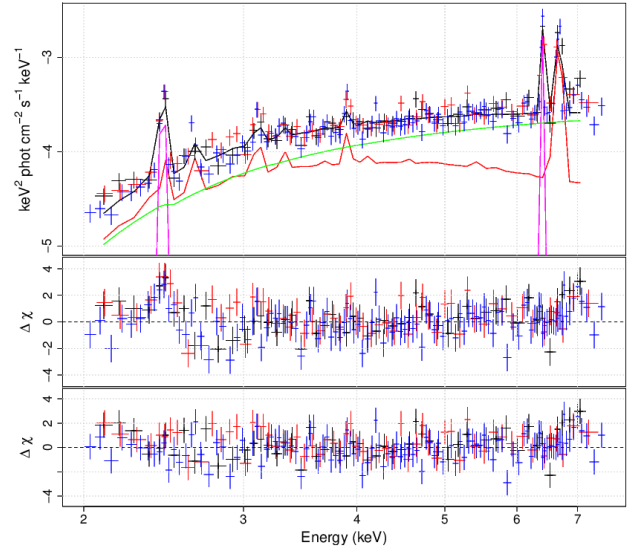


Figure 4. X-ray spectrum of the Arches cloud (cluster excluded) emission obtained with *XMM-Newton* MOS1 (black), MOS2 (red) and PN (blue) cameras in 2015. The model spectrum is represented by an absorbed thermal APEC component ($kT = 2.2$ keV, in red), non-thermal power-law continuum ($\Gamma = 1.6$, in green) with 6.4 keV fluorescent line emission (magenta), and $K\alpha$ line of He-like S at 2.45 keV (magenta), see Sect. 3.2 and Table 5 for details. Two bottom panels show residuals (data minus folded model) in terms of sigmas with error bars of size one. The middle and bottom panel demonstrate residuals of the model without and with S $K\alpha$ line included, respectively.

by C14, $N^{6.4 \text{ keV}} = 8.2 \times 10^{-6} \text{ ph cm}^{-2} \text{ s}^{-1}$ and $I_{@ 1 \text{ keV}}^{\text{pow}} = 19.3 \times 10^{-5} \text{ ph cm}^{-2} \text{ s}^{-1} \text{ keV}^{-1}$, we obtain declining factors of ~ 2.4 and ~ 1.8 , respectively.

The 2015 *XMM-Newton* data allow us to better describe the observed trend of the Arches cloud non-thermal emission. As a zero-order approach, we model the observed flux as a constant power-law normalization parameter N^{pow} followed by a linear law as a function of time $C + \alpha \times T$ after some moment of time T_{break} (C constant is derived from the continuity condition). Due to better statistics the continuum flux is better determined from the data relative to 6.4 keV line flux. The estimated best-fitting parameters for the continuum flux evolution is listed in Table 4 and the evaluated model light curve is shown in Fig. 5 (lower panel). Assuming that the 6.4 keV line flux started to decline at the same time as the continuum, we run the fitting procedure with frozen T_{break} parameter for the Fe $K\alpha$ line flux light curve as shown in the upper panel of Fig. 5. Applying the ratio between the flux normalizations $N^{6.4 \text{ keV}}/N^{\text{pow}} = (4.25 \pm 0.22) \times 10^{-2} \text{ keV}$ to the declining scale of the continuum α^{pow} we obtain the corresponding estimate $\alpha^{6.4 \text{ keV}} = (-0.55 \pm 0.09) \times 10^{-6} \text{ ph cm}^{-2} \text{ s}^{-1} \text{ year}^{-1}$ statistically consistent with that independently determined from the fit. We conclude that most of the power-law continuum was linked to the 6.4 keV line emission on a long time scale before 2015. This confirms the result obtained by C14 based on the correlation analysis. However we should note that the recent change of the EW in 2015 points towards an on-going decoupling of the continuum and line emission.

Table 4. The list of the best-fitting parameters for the constant emission flux N and linear law $C + \alpha \times T$ after T_{break} describing the evolution of the power-law non-thermal continuum and Fe $K\alpha$ flux of the Arches cloud (see Sect. 3.2).

Parameter	Units	Value	
N^*	phot keV ⁻¹ cm ⁻² s ⁻¹	power-law	Fe $K\alpha$ line
α	phot keV ⁻¹ cm ⁻² s ⁻¹ year ⁻¹	$20.78 \pm 0.71 \times 10^{-5}$	$8.84 \pm 0.34 \times 10^{-6}$
T_{break}	year	$-1.29 \pm 0.20 \times 10^{-5}$	$-0.64 \pm 0.07 \times 10^{-6}$
		2007.41 ± 0.51	2007.41 (fixed)

*) The normalization of the power-law is defined at 1 keV;

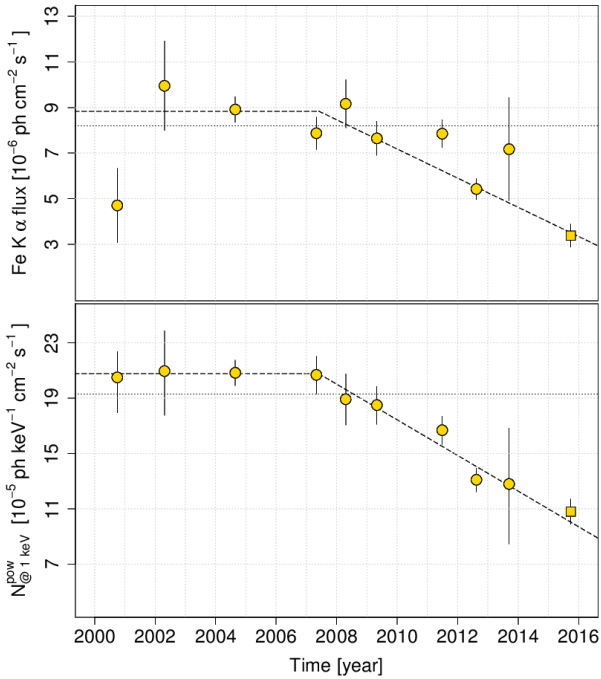


Figure 5. The evolution of the non-thermal emission of the Arches cloud as traced by Fe $K\alpha$ line flux (upper panel) and the reflection continuum (bottom panel) represented by a power-law. The declining trend of the cloud emission reported by C14 (circle points) is confirmed by the recent measurements of the current work (square points). The dotted line represents an average emission evaluated up to 2011 by C14. The fit of the constant emission followed by a linear declining trend is shown by a dashed line.

The corresponding decay time, when the flux decreases by a factor of two, was estimated to be $\tau_{1/2} = 8.05 \pm 1.28$ years. Based on the sensitivity of the current *XMM–Newton* data set and assuming constant fading rate we would expect the non-thermal emission from the Arches cluster to fall below the 2–10 keV detection limit of 2.8×10^{-14} erg cm⁻² s⁻¹ for 100 ks exposure after 2023.

3.3 *NuSTAR*: Cluster and Cloud X-ray emission

In this section we describe the spectral analysis of the Arches cluster spectrum based on dedicated *NuSTAR* observations performed with the target on-axis during two 100 ks pointings in 2015 (Table 1). We check the consistency of the spec-

Table 5. Best-fitting parameters for two models applied to *XMM–Newton* spectrum of the Arches cloud (ellipse 25'' × 59'', cluster excluded). Model 1 is identical to that used in C14; Model 2 contains extra Gaussian line at 2.45 keV.

Parameter	Unit	Model 1*	Model 2**
N_{H}	10 ²² cm ⁻²	6.51 ± 0.34	7.08 ± 0.40
kT	keV	2.2 (fixed)	2.2 (fixed)
I_{KT}	(see Sect. 3.1)	4.78 ± 0.66	4.46 ± 0.71
$E^{2.44 \text{ keV}}$	keV		2.445 ± 0.011
$N^{2.45 \text{ keV}}$	10 ⁻⁶ ph cm ⁻² s ⁻¹		12.09 ± 3.00
$EW^{2.45 \text{ keV}}$	eV		130 ± 12
$E^{6.4 \text{ keV}}$	keV	6.4 (fixed)	6.4 (fixed)
$N^{6.4 \text{ keV}}$	10 ⁻⁶ ph cm ⁻² s ⁻¹	3.06 ± 0.43	3.38 ± 0.49
$EW^{6.4 \text{ keV}}$	eV	650 ± 60	608 ± 57
Γ		1.6 (fixed)	1.6 (fixed)
$N_{\text{@1 keV}}^{\text{pow}}$	10 ⁻⁵ ph keV ⁻¹ cm ⁻² s ⁻¹	10.19 ± 0.80	10.79 ± 0.90
$\chi^2_{\text{r}}/\text{d.o.f.}$		1.54/224	1.21/222

*) WABS × (APEC + power law) + Gaussian;

**) WABS × (Gaussian + APEC + power law) + Gaussian;

tral shape of the Arches cluster with previous low-efficiency observations in 2012 when it was detected at large off-axis angles (K14). As mentioned in Sect. 2.2 we utilize FPMA data only, extracting the source spectrum from a circular region with a radius of 50'' centred at the cluster's core and including the cluster as well as the cloud emission. The background spectrum was measured in an annular region (Table 2).

To be consistent with K14 analysis we utilize three spectral models, each containing a collisionally ionized plasma emission model (APEC) representing the cluster's core thermal emission. A non-thermal emission component contains the simple power-law with a Gaussian line at 6.4 keV or cosmic-ray (CR) induced emission model or a self-consistent X-ray reflection model. Despite LECR-only emission model is almost excluded based on variability, we continue to test it because steady background level could be a result of CR heating, while most of the varying emission is due to reflection. All the emission components were subject to a line-of-sight photoelectric absorption model *wabs* in XSPEC. As the energy response of *NuSTAR* is not very sensitive for mea-

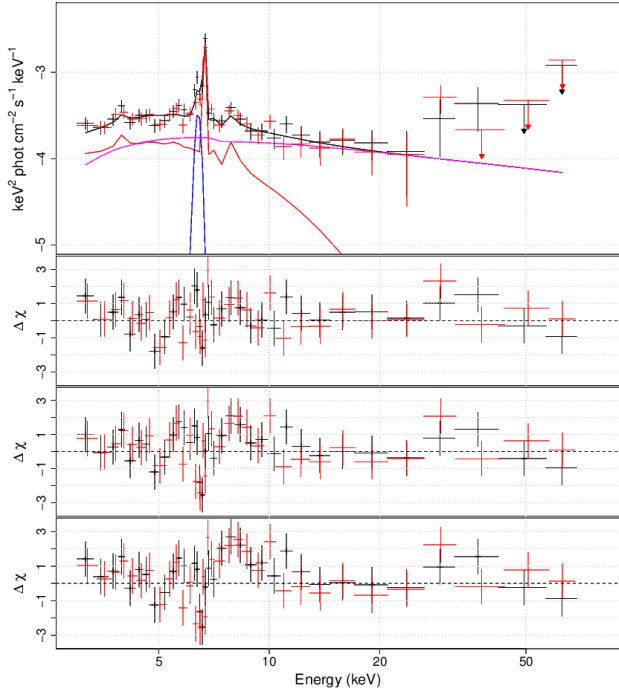


Figure 6. *Upper panel:* X-ray spectrum of the Arches cluster region as measured with FPMA during the 1st and 2nd *NuSTAR* observations, shown, respectively, in red and black data points. The lines represent best-fitting spectral model (in black) with APEC (red), power-law (magenta) and 6.4 keV Gaussian line (blue) components (Model 1 in Table 6). Given the cross-normalization factor C between the observations close to unity, only one model is shown for simplicity (1st observation). *Bottom panels* show corresponding residuals for three models listed in Table 6: power law with 6.4 keV Gaussian line, LECPp, and REFLIONX.

During the absorption column, we fixed the total absorption column at $N_{\text{H}} = 9.5 \times 10^{22} \text{ cm}^{-2}$ measured by T12 in the core of the Arches cluster. The best-fitting model parameters obtained as a result of the fitting procedure are listed in Table 6, while the *NuSTAR* spectra with model residuals are shown in Fig. 6.

This simple phenomenological model with power-law provides a reliable fit to the data with $\chi^2_{\text{r}}/\text{d.o.f.} = 0.97/364$. The temperature of the cluster’s core emission was not well constrained and found to have a relatively high value of $kT = 2.40^{+1.50}_{-0.40} \text{ keV}$ with respect to $kT = 1.76^{+0.36}_{-0.29} \text{ keV}$ measured on the *NuSTAR* data taken in 2012 with the same model (K14). The non-thermal continuum is characterized by a steeper power-law with $\Gamma = 2.41^{+0.58}_{-0.34}$ compared to 1.62 ± 0.31 in K14. The unabsorbed 3–20 keV flux of the continuum was estimated to be $F_{3-20 \text{ keV}}^{\text{pow}} = (0.56^{+0.12}_{-0.09}) \times 10^{-12} \text{ erg s}^{-1} \text{ cm}^{-2}$ compared to K14 measurement $F_{3-20 \text{ keV}}^{\text{pow}} = (1.49^{+0.26}_{-0.24}) \times 10^{-12} \text{ erg s}^{-1} \text{ cm}^{-2}$ in 2012. The drop of the continuum flux with a factor of ~ 3 in three years is stronger than a drop with a factor of 2 in eight years expected from the *XMM-Newton* data (Sect. 3.2 and 3.4). The fitting procedure determines the centroid position of Fe 6.4 keV line at $E_{6.4 \text{ keV}} = 6.34 \pm 1.12 \text{ keV}$ along with relatively low equivalent width ($EW_{6.4 \text{ keV}}$) in a range

0.25–0.56 keV compared to $EW_{6.4 \text{ keV}} \sim 1 \text{ keV}$ measured in previous works (T12, K14), confirming the lower EW measured with *XMM-Newton*. We conclude that, despite the fading of the Arches cloud emission, the non-thermal component is well constrained in 2015 observations, and still dominates the Arches cluster emission above 10 keV.

We then fitted the non-thermal emission of the cloud with the cosmic-ray induced emission model developed by T12, where the collisional ionization of the cloud by low-energy cosmic-ray (LECR) protons (LECRp) reproduces the observed 6.4 keV fluorescence line width. In contrast, the LECRe model (LECR electron) requires a metallicity $\gtrsim 3$ times the solar value to account for the measured $EW_{6.4 \text{ keV}} \sim 1 \text{ keV}$, which makes the LECRe model hardly compatible with the measured properties of the Arches cloud emission (T12, K14). We consider only the LECRp model in this work. The model depends on the LECRp path length in the ambient medium, Λ , the minimum energy of the CR particles penetrating the cloud, E_{min} , the power-law index of the CR source energy spectrum, s , the model normalization N_{LECR} and the metallicity of the X-ray emission region, Z . We fixed Λ and E_{min} parameters of the LECRp model according to T12, considering the slope s and the normalization N_{LECR} as free parameters. The model provides acceptable fit statistics ($\chi^2_{\text{r}}/\text{d.o.f.} = 1.02/367$). The power-law index $s = 2.30 \pm 0.37$ is generally higher than $s = 1.65^{+0.59}_{-0.55}$ measured by K14 with the *NuSTAR* data in 2012, however more consistent with $s = 1.9^{+0.5}_{-0.6}$ estimated by T12 for the LECRp model with the *XMM-Newton* data. The model normalization $N_{\text{LECR}} = 3.18^{+1.00}_{-0.62} \times 10^{-8} \text{ erg cm}^{-2} \text{ s}^{-1}$ implies a power injected by LECRp protons of $\sim 3 \times 10^{38} \text{ erg s}^{-1}$, which is a factor of ~ 2 less than the corresponding value measured by K14. Such a decrease rules out this model as the only contribution to the non-thermal emission up to 2012.

The third model includes the self-consistent X-ray reflection model REFLIONX which we used to describe the Arches cluster non-thermal emission in K14. REFLIONX describes the reflected spectrum for an optically thick atmosphere of constant density, illuminated by radiation with a power-law spectrum (Ross & Fabian 2005). The model predicts fluorescence lines and continuum emission. Originally developed for the surface of hot accretion disks in binary systems, REFLIONX can be well applied for cold material around the Arches cluster (K14), by fixing the ionization parameter ξ at the lowest allowed value of 10 erg cm s^{-1} . The model fits the data relatively well ($\chi^2_{\text{r}}/\text{d.o.f.} = 1.06/366$), with a somewhat steeper and less constrained photon index for the illuminating power-law spectrum $\Gamma_{\text{RX}} = 3.30^{+\infty}_{-0.19}$ compared to $\Gamma_{\text{RX}} = 2.93 \pm 0.31$ obtained by K14, which points to general softening of the spectrum confirmed by power-law model considered above.

We conclude that, similar to previous observations of the Arches cluster with *NuSTAR*, the 2015 spectral shape above $\sim 10 \text{ keV}$ is equally well described by the X-ray photoionization and CR-induced emission models, giving no direct evidence to determine the nature of the emission mechanism. Based on this, the following joint *XMM-Newton* and *NuSTAR* spectral analysis is done only for simple power-law model.

Table 6. Best-fit spectral model parameters for the Arches cluster $R = 50''$ region emission measured with *NuSTAR*.

Parameter	Unit	Model 1 *	Model 2 **	Model 3 ***
N_{H}	10^{22} cm^{-2}	9.5 (fixed)	9.5 (fixed)	9.5 (fixed)
kT	keV	$2.40^{+1.50}_{-0.40}$	$1.89^{+0.21}_{-0.15}$	$1.95^{+0.32}_{-0.17}$
I_{kT}	(see Sect. 3.1)	9.17 ± 5.28	17.46 ± 3.50	16.55 ± 3.00
$\Delta E_{6.4 \text{ keV}}$	keV	0.1 (fixed)		
$E_{6.4 \text{ keV}}$	keV	6.34 ± 1.12		
$F_{6.4 \text{ keV}}$	$10^{-6} \text{ ph cm}^{-2} \text{ s}^{-1}$	2.60 ± 1.47		
$EW_{6.4 \text{ keV}}$	eV	450 ± 150		
Γ		$2.41^{+0.58}_{-0.34}$		
$F_{3-20 \text{ keV}}^{\text{pow}}$	$10^{-13} \text{ erg cm}^{-2} \text{ s}^{-1}$	$5.58^{+1.15}_{-0.91}$		
Λ	(H-atoms cm^{-2})		5×10^{24} (fixed)	
s			2.30 ± 0.37	
E_{min}	(keV/n)		10^4 (fixed)	
N_{LECR}	($10^{-8} \text{ erg cm}^{-2} \text{ s}^{-1}$)		$3.18^{+1.00}_{-0.62}$	
Γ_{RX}				$3.30^{+\infty}_{-0.19}$
ξ	erg cm s^{-1}			10 (fixed)
I_{RX}	(10^{-5})			$7.16^{+1.01}_{-3.52}$
$\chi^2_{\text{r}}/\text{d.o.f.}$		0.97/364	1.02/367	1.06/366

* Model 1: $C \times \text{WABS} \times (\text{APEC} + \text{Gaussian} + \text{power law})$;

** Model 2: $C \times \text{WABS} \times (\text{APEC} + \text{LECR}p)$;

*** Model 3: $C \times \text{WABS} \times (\text{APEC} + \text{REFLIONX})$;

3.4 *NuSTAR* and *XMM-Newton* joint fit

In the previous sections we analysed individual *XMM-Newton* and *NuSTAR* fits to check the consistency of the spectral shape of the Arches cluster with previous measurements, and we confirmed the decrease of the net flux of the non-thermal emission of the surrounding cloud both in continuum and Fe $K\alpha$ flux. Additionally, we detected a significant decrease of the EW of the 6.4 keV line, pointing to a dramatic change of the non-thermal emission of the Arches cloud, also reflected in morphology transformation. To extract more constraints on the spectral shape of the Arches cluster emission (star cluster core and extended power-law non-thermal emission together) we present the first simultaneous *XMM-Newton*+*NuSTAR* fit on the Arches cluster complex.

Fig. 7 shows a joint *XMM-Newton* (MOS1, MOS2 and PN) and *NuSTAR* spectrum of the Arches cluster region extracted from a $R = 50''$ circular region positioned at cluster's centroid position, and the corresponding background spectrum for each instrument, containing the instrumental and astrophysical components, was extracted from the annular region around the Arches cluster (see Table 2 and Fig. 2). The way the source region is defined, the joint spectrum contains both thermal emission from the cluster and non-thermal emission from the surrounding cloud. To describe the data, we use the model containing, respectively, an APEC plasma model and a power-law continuum with a Gaussian line at 6.4 keV. We also added a cross-normalization constant between the *XMM-Newton* and *NuSTAR* data, fixing the former to unity. The joint spectrum is well described by the model with $\chi^2_{\text{r}}/\text{d.o.f.}$

$= 1.00/918$. The model parameters are listed in Table 7. The soft thermal component is not required by the fit. The best-fit cluster temperature was found at $kT = 1.95 \pm 0.14$ keV, which is in general agreement with *XMM-Newton* and *NuSTAR* data analysed separately in Sect. 3.1 and Sect. 3.3, respectively. The cross-normalization parameter $C = 0.82 \pm 0.04$ is somewhat lower than that expected from relative *XMM-Newton* and *NuSTAR* cross-calibration results (Madsen et al. 2015), which is most likely caused by the overly simplified background approximation of the *NuSTAR* data, which is contaminated by ghost-rays (Fig. 2). We tested spectral extraction with different ghost-ray-free background region, and found strong deviations in the normalization of the *NuSTAR* spectrum. For instance, using the faintest possible background region, the normalisation of the *NuSTAR* spectrum was a factor ~ 2 higher. However, these ghost-ray free background regions also introduce inaccurate deviations in the shape of the *NuSTAR* Arches cluster. Therefore, we conclude that the current annulus background region is the best possible solution, even if it is slightly overestimating the background contribution.

As seen from Table 7, we confirm that the N_{H} value chosen in the *NuSTAR* spectral analysis (Table 6), which was also used in K14, was valid. The joint fit gives the first solid measurement of the power-law Γ up to 30–40 keV and it is consistent with other molecular clouds in the CMZ (also measured by *NuSTAR*, Zhang et al. 2015; Mori et al. 2015), pointing towards a similar origin for all clouds.

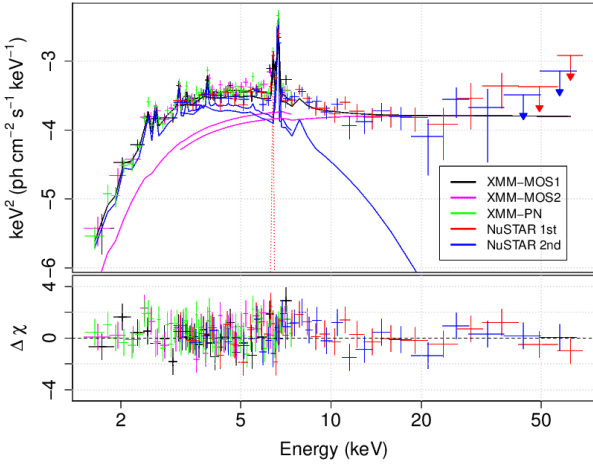


Figure 7. Joint *XMM-Newton* (MOS1, MOS2, PN) and *NuSTAR* (FPMA) spectrum of the Arches cluster region extracted from $R = 50''$ circle shown in Fig. 2. Black line represents best-fit model (Table 7), comprising thermal plasma (blue), fluorescent Fe $K\alpha$ 6.4 keV line emission (red) and non-thermal power-law continuum (magenta).

Table 7. Best-fit spectral model parameters for the Arches cluster $R = 50''$ region emission measured with *XMM-Newton* and *NuSTAR*. The model is described in XSPEC notation as WABS \times (APEC + Gaussian + power law).

Parameter	Unit	Value
N_{H}	10^{22} cm^{-2}	$9.32^{+0.86}_{-0.51}$
kT	keV	1.95 ± 0.14
l_{kT}	(see Sect. 3.1)	18.55 ± 3.00
$\Delta E_{6.4 \text{ keV}}$	keV	0.01 (fixed)
$E_{6.4 \text{ keV}}$	keV	6.38 ± 0.02
$F_{6.4 \text{ keV}}$	$10^{-6} \text{ ph cm}^{-2} \text{ s}^{-1}$	3.12 ± 0.65
$EW_{6.4 \text{ keV}}$	eV	704^{+102}_{-95}
Γ		2.03 ± 0.16
I_{pow}	$10^{-5} \text{ cm}^{-2} \text{ s}^{-1} \text{ keV}^{-1}$	$21.91^{+10.2}_{-6.90}$
C		0.82 ± 0.04
$\chi^2_{\text{r}}/\text{d.o.f.}$		1.00/918

3.5 *NuSTAR*: spatially resolved spectrum

The Arches cluster region exhibits both thermal and non-thermal emission components, originating, respectively, in the cluster’s core and nearby molecular cloud region. Despite the fact that both emission components are relatively well resolved spatially, the spectral analysis with the high resolution of *XMM-Newton* and *Chandra* still has to account for the combination of thermal and non-thermal emission components, most likely affected by projection effects. For instance, T12 model the emission of the Arches cluster region as the combination of an APEC plasma component and a non-thermal component represented by a power-law continuum and a Gaussian line at 6.4 keV.

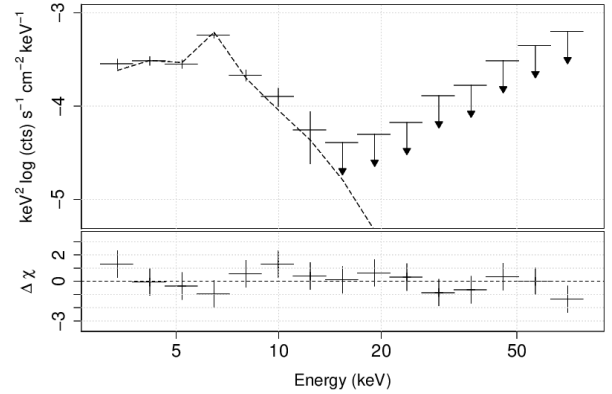


Figure 8. Spatially resolved *NuSTAR* spectrum of the Arches cluster core approximated with collisionally ionized plasma emission model APEC with temperature $kT = 2.44^{+0.40}_{-0.26}$ keV (dashed line).

Using the fact that thermal emission is concentrated in the cluster’s core, and non-thermal cloud emission is spread more widely (i.e. these components are characterized by different spatial extent or frequency as demonstrated with the use of wavelet analysis by K14), we attempt to spatially decouple the cluster and cloud hard X-ray emission in the *NuSTAR* data in order to extract their X-ray spectra. The procedure is described in Appendix B, and the results are presented in Fig. 8 and 9.

We fitted the cluster’s core emission spectrum (Fig. 8) with one APEC model subjects to a line-of-sight photoelectric absorption fixed at $N_{\text{H}} = 9.5 \times 10^{22} \text{ cm}^{-2}$. We assume that this spectrum does not include the extended non-thermal emission, so we do not need any additional components in the spectrum. This simple model provides an acceptable fit to the data with $\chi^2_{\text{r}}/\text{d.o.f.} = 0.66/13$. The only two free parameters were estimated from the fit: the temperature of the plasma $kT = 2.44 \pm 0.40$ keV and the unabsorbed 3–8 keV flux $(8.70 \pm 0.70) \times 10^{-13} \text{ erg s}^{-1} \text{ cm}^{-2}$. The cluster temperature is marginally higher, but it is still consistent with $kT = 1.6–2$ keV measured with *XMM-Newton* data, which is more sensitive to thermal emission (Sect. 3.1). In contrast, the 3–8 keV unabsorbed flux of the cluster’s thermal component is somewhat lower when compared to the corresponding value found with *XMM-Newton*: $(1.23 \pm 0.20) \times 10^{-12} \text{ erg s}^{-1} \text{ cm}^{-2}$.

Based on the 2D image spectral analysis, we assume that the spatially resolved spectrum of the Arches cloud contains the non-thermal emission only, and it is not mixed with thermal radiation of the cluster’s core. The position and width of the Gaussian line was fixed to 6.4 keV and 0.1 keV, respectively. The model gives acceptable fit statistics $\chi^2_{\text{r}}/\text{d.o.f.} = 1.02/12$ and allows for a constraint on the power-law slope $\Gamma = 2.06 \pm 0.26$ (confirming the joint *XMM-Newton* and *NuSTAR* fit results, see Sect. 3.4) and the unabsorbed 3–8 keV and 3–20 keV fluxes: $F_{3-8} = (4.92 \pm 1.00) \times 10^{-13} \text{ erg s}^{-1} \text{ cm}^{-2}$ and $F_{3-20} = (9.33 \pm 1.34) \times 10^{-13} \text{ erg s}^{-1} \text{ cm}^{-2}$. The total flux of the 6.4 keV Gaussian line was estimated to be $(1.38 \pm 0.50) \times 10^{-5} \text{ photons cm}^{-2} \text{ s}^{-1}$. Given the fit statistics and uncertainties of the model param-

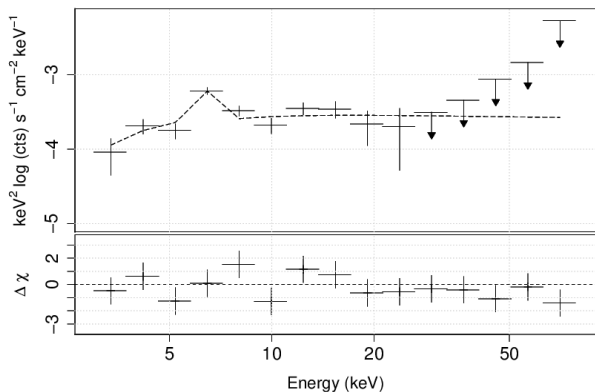


Figure 9. Spatially resolved *NuSTAR* spectrum of the Arches cloud modelled with power-law $\Gamma = 2.06 \pm 0.26$ and 6.4 keV Gaussian line.

eters, we conclude that addition of cluster’s thermal emission is not required.

We then applied a more physically motivated X-ray reflection model developed in the geometry of scattering X-ray incident photons from Sgr A* to the observer (Appendix C); however, we found that quality of the data does not allow us to constrain the reflection geometry.

4 DISCUSSION

During the long *NuSTAR* and *XMM–Newton* observations of the Arches cluster region in 2015, dedicated to monitor the emission of the molecular cloud, we observe the following distinct components in the X-ray spectra of the cluster region: an optically thin thermal plasma with a temperature $kT \sim 1.6–2.0$ keV of the stellar cluster; an additional thermal plasma component with $kT \sim 0.18–0.20$ keV of the cluster; and non-thermal emission of the cloud region characterized by a power-law continuum and fluorescent Fe $K\alpha$ 6.4 keV line. In this work we present the first solid measurement of the power-law $\Gamma \sim 2$ up to 30–40 keV. The *NuSTAR* spectrum extracted from a 50'' circular region covering the cluster and the cloud region represents a mixture of the components mentioned above. Using 2D image analysis, we decoupled spectral components (Sect. 3.5), and confirmed the power-law slope Γ of the non-thermal emission obtained with regular spectral analysis. $\Gamma \sim 2$ is consistent with other molecular clouds in the CMZ (Zhang et al. 2015; Mori et al. 2015), which points to a similar origin for all clouds. In the reflection scenario, this also means that the incident hard X-ray emission must have a power-law spectrum with $\Gamma \sim 2$ up to at least 40 keV, which adds important evidence favouring the association with past activity of Sgr A*, which exhibits a similar spectrum during X-ray flares (Barrière et al. 2014).

The morphology of the non-thermal emission of the molecular clouds near the Arches cluster reveals substructure with three bright knots to the east (E), north (N), and south (S) of the cluster’s core, marked correspondingly in Fig. 1. The current 6.4 keV line brightness distribution does not demonstrate a spatial correlation with previous morphology studies made before 2012 (Capelli et al. 2011b,

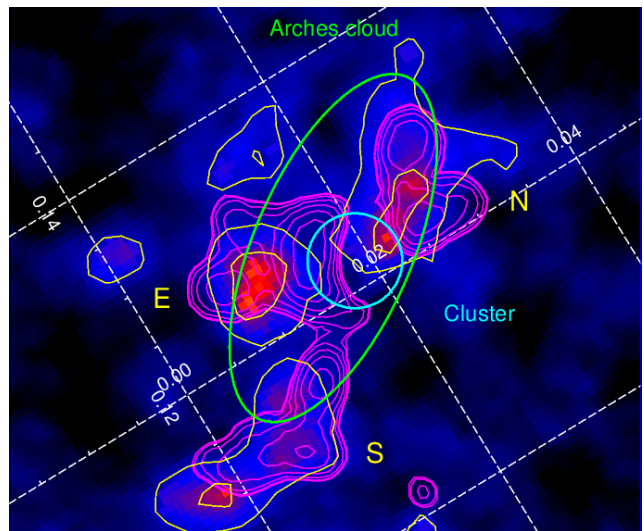


Figure 10. *XMM–Newton* $K\alpha$ line mosaic image of the Arches cluster region of Fe at 6.4 keV highlighted by yellow contours. Magenta contours show clumps of 6.4 keV emission based on low statistics map obtained in 2013 by C14.

T12), which showed mainly two bright spots to the north and to the south of the cluster (within the ellipse region). On the other hand, we found a similar pattern in the 6.4 keV map shown by C14 based on 2013 data set, which points towards a dramatic change of the morphology since 2012. To illustrate this, we show the current 6.4 keV map in Fig. 10 compared with contours of bright 6.4 keV clumps observed in 2013 by C14. A similar changes in morphology and appearance of new extended features are observed in other parts of the Galactic Centre region (e.g., Bridge, MC1, MC2, G0.11-0.11 and Sgr B2 molecular clouds, see Appendix A Ponti et al. 2010; Clavel et al. 2013). For instance, Zhang et al. (2015) revealed the substructure of the fading Sgr B2 cloud, with two compact cores, Sgr B2(M) and Sgr B2(N), and newly emerging cloud G0.66–0.13, which highlights that the illuminating front(s) propagating within this region has already started to leave its main cores. The similarities between the Arches cloud and the other molecular clouds also favour a similar reflection mechanism at the origin of their non-thermal emission. We confirm the variability seen by *XMM–Newton*, and measure, for the first time, variability of the non-thermal emission of the Arches cloud with *NuSTAR*, providing additional evidence that continuum emission above 10 keV is linked to the 6.4 keV line flux, which was not known a priori in this complex region. Strong variations of the molecular clouds in the Galactic Centre support the X-ray reflection mechanism of fluorescence observed in CMZ and reveal propagation of illuminating fronts, presumably induced by the past flaring activity of Sgr A*.

The similitude with other molecular clouds is also confirmed by the long-term variability of the non-thermal emission of the Arches cloud. The fluorescent Fe $K\alpha$ emission and hard X-ray continuum continue to demonstrate fast time variability, as discovered by C14. Thanks to the new observations with *XMM–Newton* we are able to better describe the declining trend of the cloud emission. The linear fit of the varying flux, both in Fe $K\alpha$ line and hard X-ray continuum, gives a half-time decay $\tau_{1/2} = 8.05 \pm 1.28$ years, with the

emission starting to decrease in $T_{\text{break}} = 2007.41 \pm 0.51$. Such strong variations have been observed in several other molecular clouds in the Sgr A complex (MC1, MC2 and G0.11-0.11 Capelli et al. 2012; Clavel et al. 2013), but also in the giant molecular cloud Sgr B2 (Terrier et al. 2010), which started to fade in 2001 (Inui et al. 2009) after a decade of possibly constant emission (Revnivtsev et al. 2004). However, we should note that this tentative comparison should be used with a caution: the declining trends for both the Sgr B2 region and the Arches cloud region are averaged over relatively large regions, which could include sub-structures that may vary differently (Zhang et al. 2015).

Our analysis of *XMM-Newton* and *NuSTAR* data of the Arches cloud region indicates a significant drop of the equivalent width of the Fe $K\alpha$ line $EW_{6.4 \text{ keV}} = 0.6 - 0.7 \text{ keV}$ from the average $EW_{6.4 \text{ keV}} = 0.9 \pm 0.1 \text{ keV}$ observed since 2002 (Capelli et al. 2011b, T12, K14, C14). The EW decrease can trace a relative increase of the $LECR_p$ contribution (which is known to produce a lower EW). Indeed, while its absolute contribution is expected to be constant over time, its relative contribution to the total amount of non-thermal emission should be increasing as the reflection component is decreasing. However, the drop in EW could also be due to a change in the geometry or the metallicity of the reflector. Due to the dramatic recent changes in the morphology of the 6.4 keV emission, this second explanation (or a combination of the two) should not be excluded.

In the X-ray reflection scenario, within a single cloud, the EW is only expected to increase with time (based on absorption, see e.g. Odaka et al. 2011), so a lower EW would mean that we are seeing a structure that is at a different position along the line-of-sight. The clumps of 6.4 keV line emission, visible in 2015 (and 2013), were not seen to be bright in 2000-2012, which means that reflection is still contributing to a certain extent to the faint 2015 emission and that the illuminating front is now reaching different clumps. If these new clumps are within the same cloud, this means that the illuminating event is rather short (the light curve average over the 'cloud' region is hiding faster variations) and if they are not part of the cloud, they are likely to be in a very different location along the line of sight and be illuminated by a different event.

5 SUMMARY

Recent *NuSTAR* and *XMM-Newton* observations of the molecular cloud around the Arches cluster demonstrate a dramatic change both in morphology and intensity of the non-thermal emission. Below we summarize the main results of this work.

- Despite the observed fading, the non-thermal continuum emission of the cloud is detected up to $\sim 30 - 40 \text{ keV}$. The continuum is well approximated by a power-law with $\Gamma \sim 2$, which is the first direct measurement of the Arches hard X-ray continuum, consistent with other molecular clouds measured with *NuSTAR* (Zhang et al. 2015; Mori et al. 2015)

- The relatively homogeneous morphology of the non-thermal emission traced by fluorescent Fe $K\alpha$ line has changed since 2012, revealing three bright clumps around the Arches cluster, which are detected in 2015.

- With long *XMM-Newton* observations in 2015, we confirmed the declining trend of the non-thermal emission of the cloud reported by C14.

- By fitting a simple broken linear trend to the Arches cloud emission, we showed that the constant emission of the cloud started to decline in 2007. The fading rate is consistent both in power-law continuum and 6.4 keV line flux, which indicates that most of the non-thermal continuum was linked to the fluorescent Fe $K\alpha$ 6.4 keV line emission on a long time scale. The estimated half-life time decay, $\tau_{1/2} = 8.05 \pm 1.28 \text{ years}$, is similar to that observed in several other molecular clouds in the Galactic Centre, including the giant molecular cloud Sgr B2, which adds more evidence that the same reflection mechanism is operating in both these clouds and that the main illuminating front(s) has already started to leave these clouds.

- We have obtained the non-thermal X-ray spectrum of the Arches cloud by carefully separating the signal from thermal emission of the cluster core. The spectrum is well described by a power-law continuum with $\Gamma \sim 2$ and a Gaussian line at 6.4 keV. A more physically motivated model based on Monte Carlo simulations fits the spectrum equally well; however, limited statistics does not allow for a constraint on the reflection geometry (Appendix C).

- The equivalent width of the fluorescent Fe $K\alpha$ line $EW_{6.4 \text{ keV}}$ revealed a sharp decrease to $0.6 - 0.7 \text{ keV}$ in 2015, compared to $EW_{6.4 \text{ keV}} = 0.9 \pm 0.1 \text{ keV}$ observed over 13 years since 2002. This could indicate a change in reflection to different line of sight or metallicity of the clumps or that the CR component has become more dominant.

- The measured $2 - 10 \text{ keV}$ unabsorbed total flux of the Arches cluster, $1.50_{-0.25}^{+0.30} \times 10^{-12} \text{ erg s}^{-1} \text{ cm}^{-2}$, is fully consistent with its normal state flux level observed by Capelli et al. (2011a), and no outburst from the cluster was detected during our observation in 2015.

- Using *XMM-Newton* and *NuSTAR* observations in 2015, we demonstrate (see Appendix A) a strong correlation between the 6.4 keV line flux and the hard $10 - 20 \text{ keV}$ X-ray continuum emission of the Br1 and Br2 clouds of the 'Bridge' region (Ponti et al. 2010). The emission of MC2 cloud is dim, which confirms the decreasing trend reported in earlier works (Capelli et al. 2012; Clavel et al. 2013).

ACKNOWLEDGMENTS

This work has made use of data from the *NuSTAR* mission, a project led by the California Institute of Technology, managed by the Jet Propulsion Laboratory and funded by the National Aeronautics and Space Administration, and reobservations obtained with *XMM-Newton*, an ESA science mission with instruments and contributions directly funded by ESA Member States and NASA. The research has made use of the *NuSTAR* Data Analysis Software (*nustardas*) jointly developed by the ASI Science Data Center (ASDC, Italy) and the California Institute of Technology (USA). GP acknowledges support by the Bundesministerium für Wirtschaft und Technologie/Deutsches Zentrum für Luft- und Raumfahrt (BMW/DLR, FKZ 50 OR 1408 and FKZ 50 OR 1604) and the Max Planck Society. RK acknowledges support from the Russian Basic Research Foundation (grant 16-02-00294), the Academy of Finland

(grant 300005) and hospitality of the Tuorla Observatory, and thanks Eugene Churazov for the Monte Carlo X-ray reflection model used in the paper.

APPENDIX A: SERENDIPITOUS DETECTION OF THE SGR A COMPLEX

Fig. A1 shows a part of CMZ region covered by *XMM–Newton* and *NuSTAR* observations of the Arches cluster, which allows us to capture the present state of the cloud’s surface brightness distribution in 2015. The cloud designation is taken from Clavel et al. (2013) who analysed the *Chandra* data of the Sgr A complex, in particular the ‘Bridge’ region (Ponti et al. 2010), splitting it into the two clouds Br1 and Br2, which are the brightest features in our observations. Fig. A1 demonstrates the presence of a strong correlation between the 6.4 keV line flux (*XMM–Newton*) and hard 10–20 keV X-ray continuum emission (*NuSTAR*) of Br1 and Br2. Unfortunately the region around the MC1 cloud is strongly contaminated by ghost-rays (Fig. 2). Only partly covered by the *NuSTAR* FOV, the emission of the MC2 cloud is dim, both in 6.4 keV line and hard X-ray continuum, which is in agreement with the decreasing trend reported in earlier works (Capelli et al. 2012; Clavel et al. 2013). The detailed study of the Sgr A complex based on the current *XMM–Newton* and *NuSTAR* observations will be presented in a separate paper.

APPENDIX B: X-RAY SPECTRUM EXTRACTION FROM A 2D IMAGE

In the following procedure we repeat a similar two-dimensional (2D) image analysis as done by Krivonos & Sazonov (2016), who analysed *NuSTAR* data of the local Seyfert 2 active galactic nucleus (AGN) NGC 5643 and successfully decoupled partially confused spectra of the AGN core and an ultra-luminous source located in the same galaxy.

We first combined the FPMA data from both *NuSTAR* observations into sky mosaics in 15 energy bands logarithmically covering the *NuSTAR* working energy range 3–79 keV. Each sky image was analysed with the *SHERPA* package. The spatial model of the Arches cluster includes two 2D Gaussians. The first represents the cluster’s core emission, with the position fixed at core centroid coordinates measured in K14 (see Sect. 2.2) and width fixed at 4’’ FWHM (PSF smearing effect). Similar to that, the second Gaussian was aligned with the corresponding ‘halo’ Gaussian component used in K14 to describe the cloud emission, setting the position at R.A.=17^h45^m50.62^s, Dec.=−28°49′47.17’’ and FWHM model parameter at 72’’ .4. Despite the fact that the morphology of the cloud emission has been changed since 2012, the ‘halo’ Gaussian still covers the spatial extent of the molecular cloud region. The amplitudes of the 2D Gaussians were free parameters. The background term was estimated in the annulus 70’’ < R < 130’’ shown in Fig. 2. By running the fitting procedure in each of the 15 energy bands, we extracted the detector Pulse Height Amplitude (PHA) spectrum of both spatial components. The corresponding Redistribution Matrix File (RMF), which maps from energy space

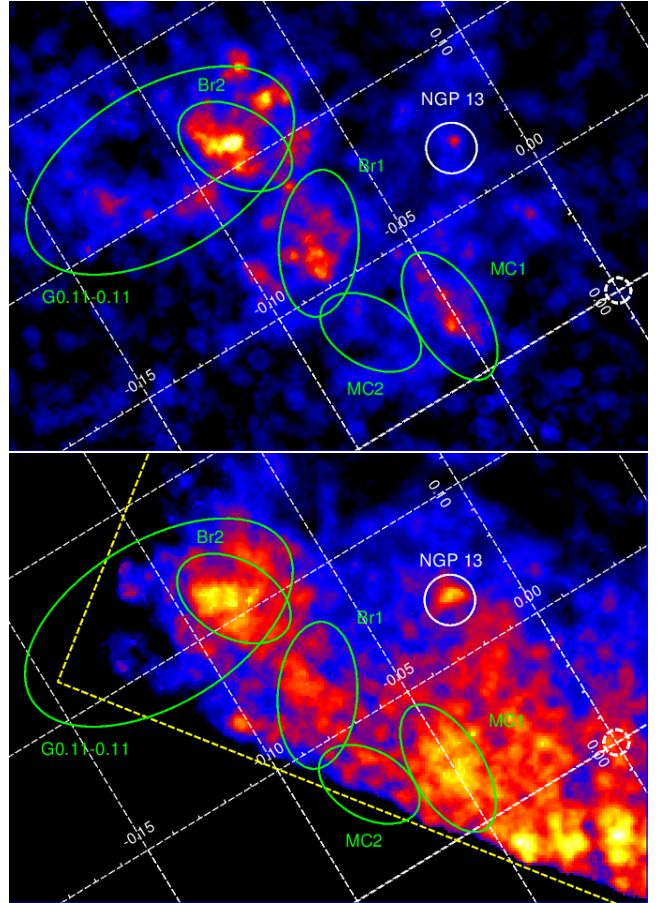


Figure A1. *Upper panel:* *XMM–Newton* image of the molecular zone complex region at 6.4 keV. *Lower panel:* *NuSTAR* image of the same sky region in 10–20 keV energy band. Green regions demonstrate the spatial extent of known illuminated clouds (Clavel et al. 2013) and white circle shows the position of hard X-ray point source NGP 13 (Hong et al. 2016). The center of the Galactic coordinates is marked by the dashed circle. Yellow dashed lines delimit edges of the *NuSTAR* image.

into PHA space, was simply adopted from standard spectral analysis with *nuproducts* (Sect. 2.2) and rebinned with *rbnmftool* of *HEASOFT* 6.19 package. Following the approach described in Krivonos & Sazonov (2016) we calibrated Auxiliary Response File (ARF) utilizing the *NuSTAR* data of a bright source with a known spectrum. To this end we used a 20 ks observation (ObsID: 80001003002) of the MeV Blazar PMN J0641-0320 with a very hard power-law spectrum of $\Gamma \approx 1$ detectable up to ~ 80 keV (Ajello et al. 2016). Here we assume that the ARF calibrated for a point-like source is suitable for the extended emission of the Arches cloud. Given the limited statistics of the *NuSTAR* Arches cluster observations, the deviations are within the uncertainties.

Spatially decoupled spectra of the Arches cluster core and extended cloud emission are shown in Fig. B1. X-ray emission of the cluster contains an excess in the 5.8–7.2 keV range, compatible with ~ 6.7 keV line and rapidly drops above ~ 10 keV as expected for thermal emission with $kT \approx 2$ keV. Non-thermal emission of the extended cloud component apparently includes excess around 6.4 keV and domi-

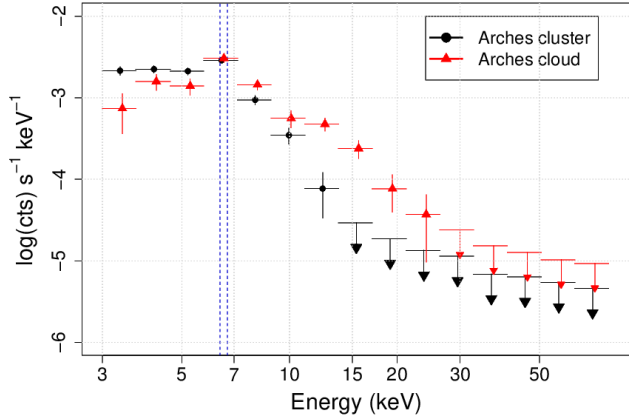


Figure B1. Spatially resolved *NuSTAR* spectra of the Arches cluster core (black) and cloud (red) X-ray emission. The position of Fe $K\alpha$ 6.4 and 6.7 keV are marked by vertical dashed lines, as in the *NuSTAR* standard spectra these two lines cannot be separated by our technique. The upper limits are 1σ errors.

nates above 10 keV. This is consistent with what was inferred from the *NuSTAR* images in 3–10, 6–7, and 10–20 keV (K14).

APPENDIX C: X-RAY REFLECTION MODEL

The X-ray reflection model, based on Monte Carlo simulations of the radiative transfer in the gas cloud, was initially developed for calculation of an X-ray albedo of the Earth atmosphere (Churazov et al. 2008). The model was later modified to the geometry more appropriate for illumination of GC molecular clouds. Namely, a uniform spherical cloud is illuminated by an external source with a given spectrum (Churazov et al. 2016). The spectrum emerging from the molecular cloud depends on several parameters: the slope (Γ) of the incident power-law spectrum, the cloud optical depth to Thomson scattering $\tau_T = \sigma_T(2n_{H_2})r$, where n_{H_2} is the number density of hydrogen molecules and r is the cloud radius, the iron abundance relative to solar, the scattering angle (θ) for photons travelling from Sgr A* to the Arches cloud and then to the observer, and the ISM line-of-sight column density toward the cloud (N_H).

In the current model setup we fixed the power-law slope of the incident Sgr A* spectrum at $\Gamma = 2$, consistent with a) what was measured above, b) Sgr B2 X-ray reflection scenarios (Revnivtsev et al. 2004; Terrier et al. 2010; Zhang et al. 2015; Walls et al. 2016), and c) observed for Sgr A* flares (Porquet et al. 2003, 2008; Nowak et al. 2012; Barrière et al. 2014). The optical depth of the cloud was not constrained by the fit ($\tau_T < 0.06$), and was fixed at the lowest value allowed by the model $\tau_T = 0.02$, which is in turn consistent with Capelli et al. (2011b) measurements $\tau_T = 0.01 - 0.03$ of the North and South bright Fe $K\alpha$ knots of the Arches cloud. The metallicity was fixed to $Z = 1.7Z_\odot$, in accordance with the whole analysis of this paper. To cover a wide range of scattering angles θ from 180° to 0° (backscattering), we built a set of eight models for different $\mu = \cos(\theta)$, ranging from -1.0 to 1.0 with step of 0.25. Fig. C1 shows fit statistics for the

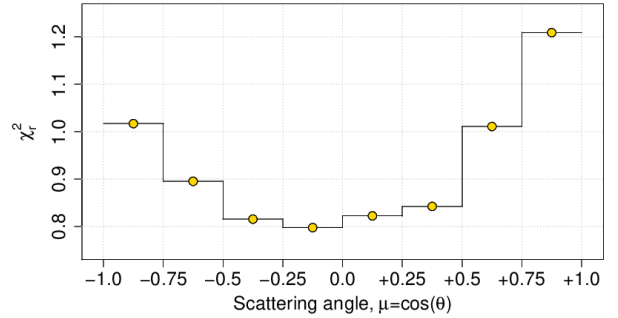


Figure C1. Reduced χ^2 fit statistics for 14 d.o.f. of the Arches cloud *NuSTAR* spectrum fitted with the X-ray reflection model as a function of scattering angle θ expressed in $\mu = \cos(\theta)$.

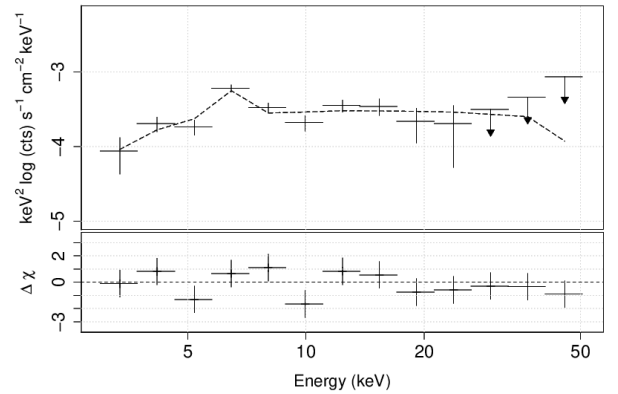


Figure C2. Spatially resolved *NuSTAR* spectrum of the Arches cloud modelled with X-ray reflection model.

models as a function of μ . As seen from the figure, the quality of the data formally allows wide range of the scattering angles θ , however revealing local extremum at $\mu = -0.25..0.0$ ($\theta = 90 - 105^\circ$), suggesting the cloud be located in or slightly in front of the Sgr A* plane. The corresponding spectral fit is shown in Fig. C2.

REFERENCES

- Ajello M., et al., 2016, *ApJ*, 826, 76
 Barrière N. M., et al., 2014, *ApJ*, 786, 46
 Bodaghee A., et al., 2014, *ApJ*, 791, 68
 Capelli, R., Warwick, R. S., Cappelluti, N., et al. 2011a, *A&A*, 525, L2
 Capelli, R., Warwick, R. S., Porquet, D., Gillessen, S., & Predehl, P. 2011b, *A&A*, 530, A38
 Capelli R., Warwick R. S., Porquet D., Gillessen S., Predehl P., 2012, *A&A*, 545, A35
 Churazov, E., Gilfanov, M., Sunyaev, R., et al. 1993, *ApJ*, 407, 752
 Churazov E., Sazonov S., Sunyaev R., Revnivtsev M., 2008, *MNRAS*, 385, 719
 Churazov E., Khabibulin I., Sunyaev R., Ponti G., 2016, *MNRAS*, submitted

- Clavel M., Terrier R., Goldwurm A., Morris M. R., Ponti G., Soldi S., Trap G., 2013, *A&A*, 558, A32
- Clavel M., Soldi S., Terrier R., Tatischeff V., Maurin G., Ponti G., Goldwurm A., Decourchelle A., 2014, *MNRAS*, 443, L129
- Degenaar, N., Wijnands, R., Miller, J. M., et al. 2015, *Journal of High Energy Astrophysics*, 7, 137
- Degenaar N., Reynolds M. T., Wijnands R., Miller J. M., Kennea J. A., Ponti G., Haggard D., Gehrels N., 2016, *ATel*, 9196,
- Dogiel, V., Cheng, K.-S., Chernyshov, D., et al. 2009, *PASJ*, 61, 901
- Dogiel V. A., Chernyshov D. O., Kiselev A. M., Cheng K.-S., 2014, *APh*, 54, 33
- Figer, D. F., Kim, S. S., Morris, M., et al. 1999, *ApJ*, 525, 750
- Figer, D. F., Najarro, F., Gilmore, D., et al. 2002, *ApJ*, 581, 258
- Freeman, P., Doe, S., & Siemiginowska, A. 2001, *Proc. SPIE*, 4477, 76
- Fruscione, A., McDowell, J. C., Allen, G. E., et al. 2006, *Proc. SPIE*, 6270,
- Harrison, F. A., Craig, W. W., Christensen, F. E., et al. 2013, *ApJ*, 770, 103
- Hong J., et al., 2016, *ApJ*, 825, 132
- Kalberla P. M. W., Burton W. B., Hartmann D., Arnal E. M., Bajaja E., Morras R., Pöppel W. G. L., 2005, *A&A*, 440, 775
- Inui T., Koyama K., Matsumoto H., Tsuru T. G., 2009, *PASJ*, 61, S241
- Koyama, K., Maeda, Y., Sonobe, T., et al. 1996, *PASJ*, 48, 249
- Krivonos R. A., et al., 2014, *ApJ*, 781, 107
- Krivonos, R., & Sazonov, S. 2016, *MNRAS*,
- Lotti, S., Natalucci, L., Mori, K., et al. 2016, *ApJ*, 822, 57
- Madsen, K. K., Harrison, F. A., Markwardt, C. B., et al. 2015, *ApJS*, 220, 8
- Markevitch M., Sunyaev R. A., Pavlinsky M., 1993, *Natur*, 364, 40
- Mori K., et al., 2015, *ApJ*, 814, 94
- Muno M. P., et al., 2004, *ApJ*, 613, 1179
- Muno M. P., et al., 2009, *ApJS*, 181, 110
- Murakami, H., Koyama, K., Sakano, M., Tsujimoto, M., & Maeda, Y. 2000, *ApJ*, 534, 283
- Nowak, M. A., Neilsen, J., Markoff, S. B., et al. 2012, *ApJ*, 759, 95
- Odaka H., Aharonian F., Watanabe S., Tanaka Y., Khangulyan D., Takahashi T., 2011, *ApJ*, 740, 103
- Ponti, G., Terrier, R., Goldwurm, A., Belanger, G., & Trap, G. 2010, *ApJ*, 714, 732
- Ponti G., Morris M. R., Terrier R., Goldwurm A., 2013, *ASSP*, 34, 331
- Ponti, G., Bianchi, S., Muñoz-Darias, T., et al. 2015, *MNRAS*, 446, 1536
- Porquet, D., Predehl, P., Aschenbach, B., et al. 2003, *A&A*, 407, L17
- Porquet, D., Grosso, N., Predehl, P., et al. 2008, *A&A*, 488, 549
- Revnivtsev, M. G., Churazov, E. M., Sazonov, S. Y., et al. 2004, *A&A*, 425, L49
- Ross, R. R., & Fabian, A. C. 2005, *MNRAS*, 358, 211
- Ryu S. G., Nobukawa M., Nakashima S., Tsuru T. G., Koyama K., Uchiyama H., 2013, *PASJ*, 65,
- Seifina E., Titarchuk L., 2012, *ApJ*, 747, 99
- Snowden S. L., Mushotzky R. F., Kuntz K. D., Davis D. S., 2008, *A&A*, 478, 615
- Sunyaev R. A., Markevitch M., Pavlinsky M., 1993, *ApJ*, 407, 606
- Sunyaev, R., & Churazov, E. 1998, *MNRAS*, 297, 1279
- Tatischeff, V., Decourchelle, A., & Maurin, G. 2012, *A&A*, 546, A88
- Terrier, R., Ponti, G., Bélanger, G., et al. 2010, *ApJ*, 719, 143
- Terrier R., et al. 2017, in prep
- Tsujimoto, M., Hyodo, Y., & Koyama, K. 2007, *PASJ*, 59, 229
- Valinia A., Tatischeff V., Arnaud K., Ebisawa K., Ramaty R., 2000, *ApJ*, 543, 733
- Walls M., Chernyakova M., Terrier R., Goldwurm A., 2016, *MNRAS*, 463, 2893
- Wang, Q. D., Dong, H., & Lang, C. 2006, *MNRAS*, 371, 38
- Wik D. R., et al., 2014, *ApJ*, 792, 48
- Yusef-Zadeh, F., Law, C., Wardle, M., et al. 2002, *ApJ*, 570, 665
- Zhang S., et al., 2015, *ApJ*, 815, 132

This paper has been typeset from a $\text{\TeX}/\text{\LaTeX}$ file prepared by the author.